RSC Advances

PAPER

View Article Online
View Journal | View Issue

Cite this: *RSC Adv.*, 2016, **6**, 104433

Anomalous Hall effect in tetragonal antiperovskite $GeNFe_3$ with a frustrated ferromagnetic state†

X. C. Kan,[ab] B. S. Wang,*[a] L. Zu,[ab] S. Lin,[a] J. C. Lin,[a] P. Tong,[a] W. H. Song*[a] and Y. P. Sun[acd]

Received 20th June 2016
Accepted 17th October 2016

DOI: 10.1039/c6ra15976a

www.rsc.org/advances

We report observed anomalous Hall effect (AHE) behavior in the antiperovskite compound $GeNFe_3$ with a tetragonal symmetry. The anomalous Hall coefficient R_H was estimated and exhibits a broad peak near the ferromagnetic (FM)–paramagnetic (PM) phase transition, and reduces to zero in the PM phase. The sign of the ordinary Hall coefficient R_0 changes sharply as a function of temperature, which provides evidence for the switching of different domain carriers. The relationship between the R_H and ρ_{xx} data was also plotted using the scaling law $R_H = a\rho_{xx0} + b\rho_{xx}^{\gamma}$, and the parameter γ is found to be about 0.99. These results suggest that the mechanism of the AHE for tetragonal $GeNFe_3$ is mainly due to skew scattering. This finding enriches the understanding of the AHE mechanism for antiperovskite compounds, and the unusual mechanism for $GeNFe_3$ is considered to be closely related to the unique tetragonal crystal structure and frustrated FM ground state of antiperovskite compounds.

I Introduction

The Anomalous Hall Effect (AHE), an electron transport phenomenon that relies on the spin–orbit coupling effect, has attracted considerable interest in recent years due to its intrinsic physics and device applications.[1–4] For example, in the orthorhombic phase of Mn_3Sn, one of the three moments in each Mn triangle is parallel to the local easy-axis. The canting configuration of the other two spins towards the local easy-axis leads to an antiferromagnet which has a non-collinear 120 degree spin order. These unique characteristics were considered to be the origin of the large anomalous Hall conductivity.[2] Usually, the transverse resistivity (Hall resistivity) ρ_{xy} consists of two contributions ($\rho_{xy} = R_0H + R_HM_S$) where H is the magnetic induction, M_S is the saturation magnetization and R_0 (R_H) is the ordinary (anomalous) Hall coefficient. The R_0H term represents the ordinary Hall resistivity which originates from the Lorentz force, and the R_HM_S term represents the anomalous Hall resistivity (ρ_{AH}). The mechanism of the AHE could be obtained from either intrinsic or extrinsic mechanisms, which usually consist of skew scattering and side-jump contributions.[5–7] The intrinsic mechanism (R_H (or ρ_{AH}) $\propto \rho_{xx}^2$, where ρ_{xx} is the longitudinal resistivity) originates from the band filling effects,[5] while the skew scattering[6] ($R_H \propto \rho_{xx}$) and side-jump[7] ($R_H \propto \rho_{xx}^2$) contributions arise from the spin–orbit interactions. The scaling law between R_H (or ρ_{AH}) and ρ_{xx} is described as $R_H = a\rho_{xx0} + b\rho_{xx}^{\gamma}$ in order to identify the AHE mechanism.[3]

Recently, the antiperovskite structural Fe-based nitride $ANFe_3$ (A = Ga, Al, Sn, Zn, Cu, In *etc.*) has attracted attention because of its potential applications in spintronic devices.[8–10] As a typical case, Fe_4N has attracted considerable interest as one candidate for a ferromagnetic (FM) electrode.[11] Recent studies on Fe_4N have revealed that side-jump and intrinsic contributions are the possible and underlying mechanisms of the AHE.[12] Similarly, the Mn-based nitride alloy Mn_4N has also been reported to exhibit an AHE, and its main mechanism is side-jump scattering.[12,13] As we know, crystal structure plays an important role in determining the magnetic and electronic properties of compounds, which significantly influence the AHE for a special material, and the scattering mechanism of AHE might show a strong dependence on material systems. Different from the reported antiperovskite compounds which have cubic crystal structures, we focused on the tetragonally structured $GeNFe_3$ which has a space group of $I4/mcm$.[14] Compared with the cubic phase, the tetragonal phase is much more complicated in microstructure and in terms of crystallographic sites occupied by iron atoms, indicating that $GeNFe_3$ is an excellent candidate for investigating the mechanism of the AHE. Meanwhile, we also noticed that there have been no reports about the physical properties of $GeNFe_3$ until now, except for those providing structural information.[14] Thus, it is important to study the AHE of the Fe-based nitride $GeNFe_3$ and to obtain a comprehensive understanding of the possible AHE mechanisms. In this work,

[a]*Key Laboratory of Materials Physics, Institute of Solid State Physics, Chinese Academy of Sciences, Hefei 230031, China. E-mail: bswang@issp.ac.cn; whsong@issp.ac.cn; Fax: +86-551-559-1434; Tel: +86-551-559-1436*

[b]*University of Science and Technology of China, Hefei 230026, China*

[c]*High Magnetic Field Laboratory, Chinese Academy of Sciences, Hefei 230031, China*

[d]*Collaborative Innovation Center of Advanced Microstructures, Nanjing University, Nanjing, 210093, China*

† Electronic supplementary information (ESI) available. See DOI: 10.1039/c6ra15976a

we observed the AHE in tetragonal $GeNFe_3$ and the mechanism was proposed, using the scaling law, to be due to extrinsic contributions (skew scattering).

II Experimental details

Polycrystalline $GeNFe_3$ was synthesized by the solid-state reaction of GeO_2 (5 N) and Fe (3 N). The starting materials were weighed according to the stoichiometric ratio (the molar ratio of GeO_2 to Fe is 1 : 3), thoroughly ground, and then annealed at 923 K for 10 hours in a flowing NH_3 atmosphere (500 cc min^{-1}). After quenching to room temperature, the products were pulverized, mixed, pressed into pellets, and then annealed again for 10 hours in a flowing NH_3 atmosphere (500 cc min^{-1}) in order to obtain the homogeneous samples. X-ray diffraction (XRD) studies were conducted at room temperature using an X-ray diffractometer with Cu Kα radiation (PHILIPS, $\lambda_{\alpha1} = 1.5406$ Å, $\lambda_{\alpha2} = 1.5443$ Å, and Kα1 : Kα2 = 2 : 1) to determine the crystal structure and phase purity. The chemical compositions of the samples were examined using an energy-dispersive X-ray spectrometer (EDS). Magnetic measurements were performed on a quantum design superconducting quantum interference device magnetometer (SQUID-5T). The electrical transport properties were measured using the standard four-probe method on a commercial quantum design physical property measurement system (PPMS-9T). Hall measurements were performed by polishing the sample to a thickness of ~0.1 mm and using a five-probe method on the PPMS-9T.

III Results and discussion

Fig. 1(a) shows the sketched crystal structure of the anti-perovskite compound $GeNFe_3$. In this compound, Ge and N are located at the Wyckoff sites 4*b* (0, 0.5, 0.25) and 4*c* (0, 0, 0), respectively, and Fe occupies the two non-equivalent sites, namely, the Wyckoff sites 4*a* (0, 0, 0.25) for Fe1 and 8*h* (0.23, 0.73, 0) for Fe2, as shown in the top map of Fig. 1(a). The symmetries of the occupied Wyckoff sites are also given (4*a*: 4 2 2; 4*b*: −4 2 *m*; 4*c*: 4/*m*; and 8*h*: *m*. 2*m*). In the bottom map of Fig. 1(a), along the *c* axis direction, the atoms Ge, N, and Fe1 lie in a straight line. However, for atom Fe2, it is non-linear and there is a perturbation along the *c* axis direction. Fig. 1(b) presents the Rietveld refined powder XRD pattern for $GeNFe_3$ at approximately room temperature. The values of overall thermal parameter *B* and isotropic displacement parameter B_{iso}, obtained by using the refined Rietveld technique, are 0 and 0.9 respectively. All the diffraction peaks can be well described by the tetragonal symmetry of the compound (space group: *I*4/*mcm*). The refined lattice parameters, obtained by using the standard Rietveld technique, are $a = 5.3143 \pm 0.0004$ Å and $c = 7.7352 \pm 0.0007$ Å, and are consistent with the previous results,[14] which indicates the sample is of good quality and that the nitrogen content is close to 1. In addition, the detected result of EDS is plotted in the inset of Fig. 1(b). The actual atom number ratio of GeO_2 to Fe is 0.98 : 3. However, the content of light element N can not be detected correctly by EDS.

Fig. 2(a) illustrates the temperature dependence of the longitudinal resistivity ρ_{xx} for $GeNFe_3$ at zero magnetic field. Below 27 K, the low temperature resistivity can be well fitted by the formula $\rho_{xx}(T) = \rho_{xx0} + AT^2$ (ρ_{xx0} and *A* represent the residual resistivity and T^2-term coefficient of the resistivity, respectively), as shown in the inset of Fig. 2(a), which indicates a Fermi liquid behavior.[15] Above 27 K, $\rho_{xx}(T)$ data shows a gradual slope change at around 80 K, which is a signal of a magnetic transition according to the previous investigations.[15] Apart from the transition, the $\rho_{xx}(T)$ curve is almost linearly dependent on the temperature (27–70 K and 95–195 K), which indicates that electron–phonon scatterings exceed the electron–electron scatterings in these temperature ranges. The magnetic transition temperature is determined to be ~80 K from the intersection between the two fitting straight lines, which is the same as the temperature of the FM–paramagnetic phase transition as shown in Fig. S1(a).† However, upon decreasing the temperature, the number of phonons decreases sharply and the phonon scatterings weaken accordingly. The electron–electron scatterings are dominant. Meanwhile, the ρ_{xx} values at 0 T and 5 T were measured and plotted in Fig. 2(b). The magnetoresistance (MR), defined by $MR = (\rho_H - \rho_0)/\rho_0$, was estimated at around T_c and

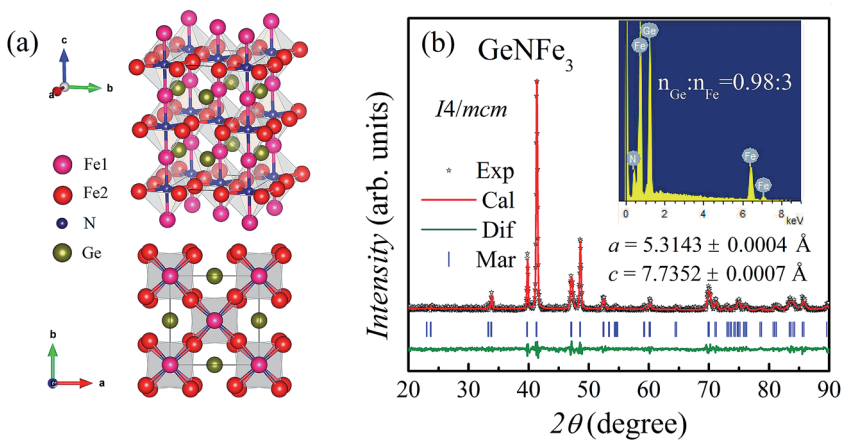

Fig. 1 (a) Crystal structure of $GeNFe_3$; (b) Rietveld refined XRD patterns for $GeNFe_3$.

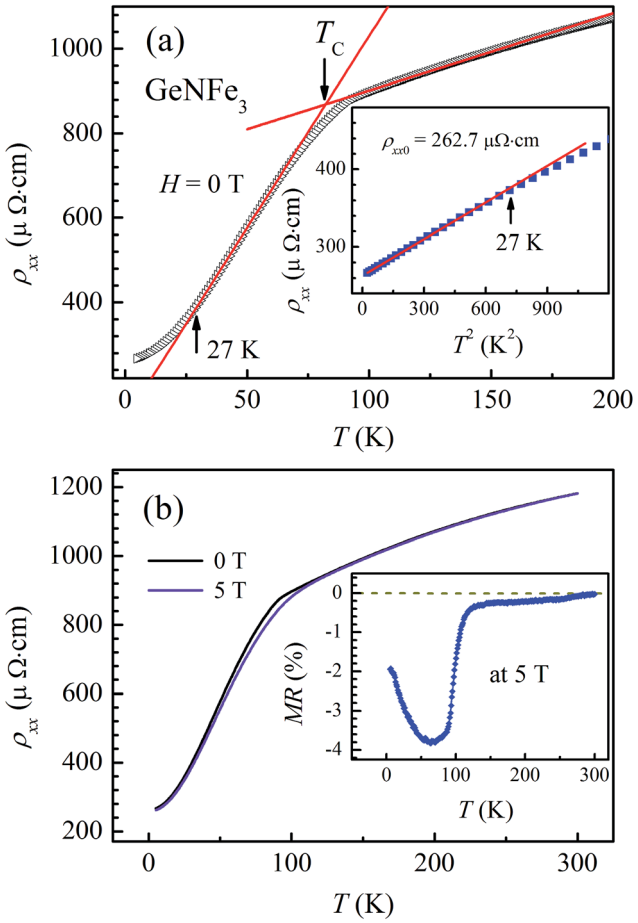

Fig. 2 (a) Temperature dependence of resistivity $\rho_{xx}(T)$ for $GeNFe_3$ at zero field. Inset shows $\rho_{xx}(T)$ *vs.* T^2 at zero field and its linear fitting to lower temperature data; (b) $\rho_{xx}(T)$ curves at 0 and 50 kOe. Inset shows the values of MR *vs.* T at 50 kOe.

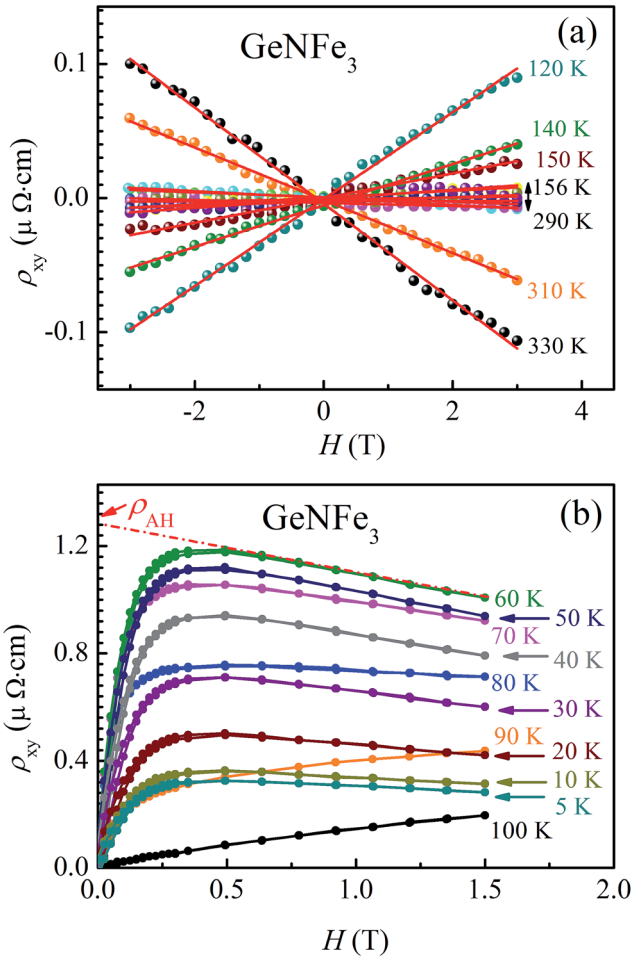

Fig. 3 Magnetic field dependence Hall resistivity curves $\rho_{xy}(H)$ at several temperatures: (a) 330 to 120 K. (b) 100 to 5 K. The red lines are the linear fittings.

was found to be about −4%, as shown in the inset of Fig. 2(b). Such a small negative MR can be largely attributed to the magnetic scatterings, similar to that of $GaCMn_3$ near its second-order transition at around 250 K.[16]

In order to investigate the AHE of $GeNFe_3$, the magnetic field dependent Hall resistivity curves $\rho_{xy}(H)$ at different temperatures were plotted as shown in Fig. 3. Obviously, in Fig. 3(a), all the data have collapsed into a straight line for each temperature from 330 K to 120 K, which suggests ordinary Hall effect behavior. As the temperature decreases ($T \leq 100$ K), the $\rho_{xy}(H)$ curves deviate from a linear relationship (Fig. 3(b)) and AHE signals are observed. The AHE signals can be analyzed using the following expression: $\rho_{xy} = R_0H + R_HM_S$, where R_HM_S (ρ_{AH}) is the anomalous Hall resistivity. As shown in Fig. 3(b), the high-field portions of the $\rho_{xy}(H)$ curves are fitted with a linear function and then extrapolated to the $H = 0$ axes to obtain ρ_{AH}.

Fig. 4(a) presents the evolution of $\rho_{AH}(T)$ data as a function of temperature. One can see that the AHE resistivity $\rho_{AH}(T)$ is positive over the entire temperature range, indicating that the skew scattering mechanism dominates the AHE in tetragonal $GeNFe_3$.[17] Meanwhile, we notice that the $\rho_{AH}(T)$ quickly increases with increasing temperature and reaches a peak value at 60 K, and then decreases with further increasing temperature. The appearance of the $\rho_{AH}(T)$ peak may be caused by competition between magnetic order and magnetic disorder due to the introduction of impurity scattering. Meanwhile, as shown in Fig. S1(a),† the zero-field cooling curve also shows a maximum value at around 60 K, similar to that of the $\rho_{AH}(T)$ curve. This suggests that the frozen temperatures appear due to the magnetic competition. To obtain the anomalous Hall coefficient R_H, isothermal $M(H)$ curves at different temperatures from 100 K to 5 K were measured and plotted in Fig. 4(b). The M_S value can be extracted from Fig. 4(b) by extrapolating the high-field data from the positive field to the zero field.

Finally, the $R_S(T)$ values are obtained from the equation $R_S(T) = \rho_{AH}(T)/M_S(T)$ and the results are shown in Fig. 5(a). For the sake of contrasting analysis, Fig. 5(a) also presents the ordinary Hall coefficient R_0 values, which are obtained from the equation $R_0 = \rho_{xy}/H$ using the data from Fig. 3(a), and from the equation $R_0 = (\rho_{xy} - \rho_{AH})/H$ using the data from Fig. 3(b). The obtained R_0 values are an order of magnitude lower than those of R_H. On cooling, the sign of R_0 changes from negative (for $T >$

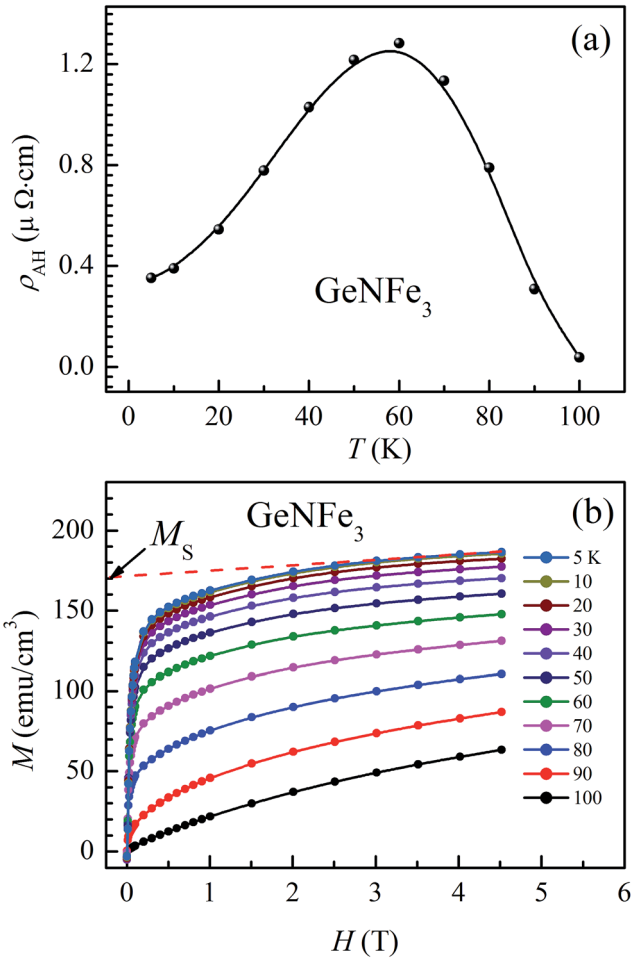

Fig. 4 (a) AHE resistivity $\rho_{AH}(T)$ as a function of temperature for $GeNFe_3$. (b) The initial isothermal magnetization $M(H)$ curves from 100 to 5 K.

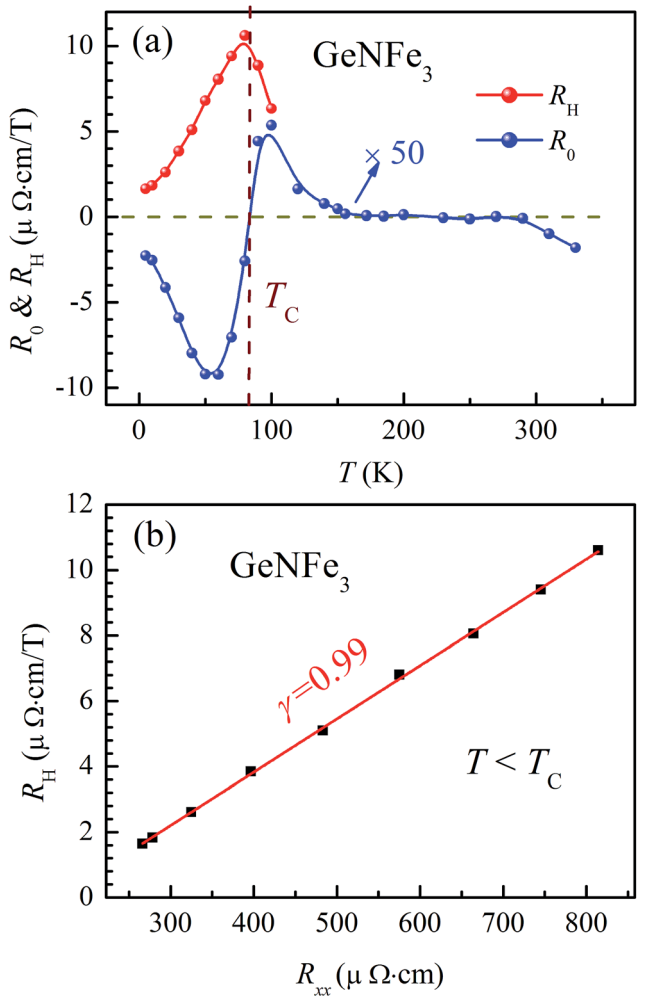

Fig. 5 (a) Temperature dependence of the ordinary Hall coefficient R_0 and the anomalous Hall coefficient R_H. (b) The ρ_{xx} dependencies of R_S. The red line is fitted using the scaling law $R_H = a\rho_{xx0} + b\rho_{xx}^{\gamma}$.

200 K) to positive (for $T_c < T < 200$ K), then to negative again (for $T < T_c$). In general, the negative and positive R_0 values are attributed to electron-like and hole-like transport, respectively. By contrast, a peak value of R_S is observed in the vicinity of T_c, which is far away from 60 K, as shown in the ρ_{AH} data of Fig. 4(a), which suggests that the influence of the M_S on ρ_{AH} can not be negligible. To clarify the mechanism of the AHE in tetragonal $GeNFe_3$, the scaling law between R_H and ρ_{xx} is given as $R_H = a\rho_{xx0} + b\rho_{xx}^{\gamma}$,[3] where the first term is the residual resistivity (ρ_{xx0}), obtained from the different contributions to the measured AHE transport data. For the second term, the parameter γ is a fitting result obtained from the AHE data. When $\gamma = 1$, the skew scattering mechanism is valid. When $\gamma = 2$, both scattering-dependent side jump and scattering-independent intrinsic mechanisms are accepted. The intermediate values $1 < \gamma < 2$ indicate a combination of the above mechanisms.[3,12] Fig. 5(b) shows the ρ_{xx} dependencies of R_H, where all the data can be well fitted by the scaling law $R_H = a\rho_{xx0} + b\rho_{xx}^{\gamma}$. The obtained value of the parameter $\gamma \sim 0.99$ indicates that the skew scattering mechanism dominates the AHE in $GeNFe_3$. The AHE mechanism of $GeNFe_3$ is quite different from that of Fe_4N, in which side-jump scattering and intrinsic contributions are responsible for the AHE.[12]

Although AHE materials have been discovered in many different systems, their mechanisms are different and show a strong dependence on the material systems. For example, in $Nd_2Mo_2O_7$,[1] the AHE is attributed to an intrinsic mechanism which is associated with the spin chirality and associated Berry phase. In antiperovskite Mn_4N films,[13] extrinsic contributions or side-jump scattering are the possible origins. Some typical AHE materials, such as Rh_2MnGe films, $Ge_{1-x-y}Pb_xMn_yTe$, and $Sb_{2-x}Cr_xTe_3$, are dominated by skew scattering mechanisms.[18–20] In Rh_2MnGe films,[18] the origin of the AHE mechanism was suggested to be spin–orbit interaction. In $Ge_{1-x-y}Pb_xMn_yTe$,[19] its cluster-glass state yields strong magnetic competition, which is related to the giant spin-splitting of the valence band, and which is the reason for the skew scattering mechanism of the AHE. In $Sb_{2-x}Cr_xTe_3$,[20] the skew scattering mechanism suggests that the AHE is disorder driven rather than an intrinsic property related to the band structure. By comparison, as mentioned above, the present

results also indicate that the frustrated FM state in $GeNFe_3$ generates magnetic competition amongst the different magnetic interactions, which may be the major reason for the skew scattering mechanism of the AHE, similar to $Ge_{1-x-y}Pb_xMn_yTe$.[19] Another possible origin is associated with the distorted crystal structure of $GeNFe_3$. Different from cubic symmetry, there is a perturbation of atom Fe2 along the *c* axis (Fig. 1(a)). These results are correlated with the strength of the spin–orbit interaction. Thus, it can be concluded that the skew scattering mechanism should be responsible for the AHE in $GeNFe_3$.

IV Conclusions

In summary, the anomalous Hall Effect was investigated in antiperovskite $GeNFe_3$. The sign of the ordinary Hall coefficient (R_0) changes as the temperature increases, indicating that the type of carrier changes. R_H (ρ_{xx}) data follows the scaling law $R_H = a\rho_{xx0} + b\rho_{xx}$. Our results indicate that the skew scattering mechanism dominates the AHE in tetragonal $GeNFe_3$.

Acknowledgements

This work is supported by the National Key Basic Research Program under contract No. 2011CBA00111 and the National Natural Science Foundation of China under contract No. 51371005, 51171177, 11174288, 11174295, and 51301167.

References

1 Y. Taguchi, Y. Oohara, H. Yoshizawa, N. Nagaosa and Y. Tokura, *Science*, 2001, **291**, 2573.
2 S. Nakatsuji, N. Kiyohara and T. Higo, *Nature*, 2015, **527**, 212.
3 N. Nagaosa, J. Sinova, S. Onoda, A. H. MacDonald and N. P. Ong, *Rev. Mod. Phys.*, 2010, **82**, 1539.
4 J. G. Checkelsky, M. Lee, E. Morosan, R. J. Cava and N. P. Ong, *Phys. Rev. B: Condens. Matter Mater. Phys.*, 2008, **77**, 014433.
5 D. Z. Hou, Y. F. Li, D. H. Wei, D. Tian, L. Wu and X. F. Jin, *J. Phys.: Condens. Matter*, 2012, **24**, 482001.
6 J. Smit, *Physica*, 1958, **24**, 39.
7 L. Berger, *Phys. Rev. B: Solid State*, 1970, **2**, 4559.
8 W. Mi, Z. Guo, X. Feng and H. Bai, *Acta Mater.*, 2013, **61**, 6387.
9 Y. Komasaki, M. Tsunoda, S. Isogami and M. Takahashi, *J. Appl. Phys.*, 2009, **105**, 07C928.
10 K. Sunaga, M. Tsunoda, K. Komagaki, Y. Uehara and M. Takahashi, *J. Appl. Phys.*, 2007, **102**, 013917.
11 S. Kokado, N. Fujima, K. Harigaya, H. Shimizu and A. Sakuma, *Phys. Rev. B: Condens. Matter Mater. Phys.*, 2006, **73**, 172410.
12 Y. Zhang, W. B. Mi, X. C. Wang and X. X. Zhang, *Phys. Chem. Chem. Phys.*, 2015, **17**, 15435.
13 M. Meng, S. X. Wu, L. Z. Ren, W. Q. Zhou, Y. J. Wang, G. L. Wang and S. W. Li, *Appl. Phys. Lett.*, 2015, **106**, 032407.
14 H. Boller, *Monatsh. Chem.*, 1968, **99**, 2444.
15 B. S. Wang, J. C. Lin, P. Tong, L. Zhang, W. J. Lu, X. B. Zhu, Z. R. Yang, W. H. Song, J. M. Dai and Y. P. Sun, *J. Appl. Phys.*, 2010, **108**, 093925.
16 B. S. Wang, P. Tong, Y. P. Sun, L. J. Li, W. Tang, W. J. Lu, X. B. Zhu, Z. R. Yang and W. H. Song, *Appl. Phys. Lett.*, 2009, **95**, 222509.
17 S. L. Jiang, X. Chen, X. J. Li, K. Yang, J. Y. Zhang, G. Yang, Y. W. Liu, J. H. Lu, D. W. Wang, J. Teng and G. H. Yu, *Appl. Phys. Lett.*, 2015, **107**, 112404.
18 M. Emmel and G. Jakob, *J. Magn. Magn. Mater.*, 2015, **381**, 360.
19 A. Podgórni, L. Kilanski, M. Górska, R. Szymczak, A. Reszka, V. Domukhovski, B. J. Kowalski, B. Brodowska, W. Dobrowolski, V. E. Slynko and E. I. Slynko, *J. Alloys Compd.*, 2016, **658**, 265.
20 J. S. Dyck, Č. Drašar, P. Lošťák and C. Uher, *Phys. Rev. B: Condens. Matter Mater. Phys.*, 2005, **71**, 115214.